

## Quantitative Study of Compositional Uniformity and Interfacial Strain in InAs/InAs<sub>1-x</sub>Sb<sub>x</sub> Type-II Superlattices

J. Lu<sup>1,2</sup>, X.-M. Shen<sup>1,2</sup>, Y.-H. Zhang<sup>1,3</sup> and D.J. Smith<sup>1,4</sup>

<sup>1</sup>. Center for Photonic Innovation, Arizona State University, Tempe, AZ 85287, USA

<sup>2</sup>. School for Engineering of Matter, Transport and Energy, Arizona State University, Tempe, AZ, USA

<sup>3</sup>. School of Electrical, Computer and Energy Engineering, Arizona State University, Tempe, AZ, USA

<sup>4</sup>. Department of Physics, Arizona State University, Tempe, AZ, USA

For infrared photo-detection in mid-wavelength and long-wavelength range, mercury cadmium telluride (MCT) semiconductor alloys remain the most widely used material system despite its major disadvantages of intrinsic Auger recombination and small effective mass. Type-II superlattices (T2SL) have been proposed as possible alternatives to MCT because they may overcome these problems by flexible and more controllable band structure engineering through SL layer thickness/composition and coherent interfacial strain, along with other benefits such as higher mechanical strength and lower cost [1,2]. InAs/Ga<sub>1-x</sub>In<sub>x</sub>Sb T2SL, the most studied III-V T2SL material system, suffers from short minority carrier lifetime possibly due to Shockley-Reed-Hall recombination, whereas the more recent Ga-free T2SL InAs/InAs<sub>1-x</sub>Sb<sub>x</sub> has demonstrated significantly improved minority carrier lifetime [3]. This current study uses extensive quantitative characterization of SL layers with nm-scale spatial resolution to explore possible performance-limiting factors: period thickness/composition variation and interfacial strain.

The InAs/InAs<sub>1-x</sub>Sb<sub>x</sub> T2SLs studied here were grown on unintentionally doped (001) GaSb substrates using MBE [3]: 58 periods of SLs were sandwiched by two 10nm AlSb barrier layers at bottom and top, with each SL period comprised of nominally 6.8nm InAs and 1.8nm InAs<sub>0.6</sub>Sb<sub>0.4</sub> (Fig. 1). Fitting of (004)  $\omega$ - $2\theta$  high-resolution XRD patterns gave average SL periods of 8.5nm and Sb composition of 34% in the InAs<sub>1-x</sub>Sb<sub>x</sub> layers, which are close to the design values. However asymmetric SL peaks (Fig. 2) suggest variations in period thickness, and possible Sb composition fluctuations throughout the total SL stack. Cross-sectional TEM samples with  $\langle 110 \rangle$  and  $\langle 210 \rangle$  zone axes were prepared by dimple grinding followed by 2.3keV Ar<sup>+</sup> ion milling with liquid nitrogen cooling to minimize ion mill damage.

Imaging using TEM (JEOL 4000EX) and aberration-corrected STEM (AC-STEM, JEOL ARM200F) revealed variation of period thickness along the growth direction (Fig. 3), while strain analysis using geometric phase analysis (GPA) showed asymmetric interface with InAs-on-InAsSb interface broadening (Fig. 4) suggesting possible Sb diffusion (as also reported in [4]). EELS spectrum imaging provides local quantitative chemical composition with slightly deteriorated yet high enough spatial resolution and thus allow determination of Sb% throughout the SL stack as well as the interface abruptness.

The strain profile across SL interfaces was investigated using convergent beam electron diffraction (CBED) by fitting the positions of high-order Laue zone (HOLZ) lines in the transmitted disks of experimentally recorded and simulated diffraction patterns. To achieve nm-scale local strain measurement with sensitivity of ( $\Delta a/a$ )~0.1%, accelerating voltage and specimen thickness were determined, respectively, by fitting experimental and simulated HOLZ lines positions of GaSb buffer layer (assuming bulk GaSb lattice constants), and short camera length zone axis CBED patterns. All

kinematical and Bloch wave dynamical fitting procedures were performed assuming tetragonal distortion. Zone axis of  $\langle 210 \rangle$  instead of  $\langle 110 \rangle$  was used to avoid strong dynamical scattering and improve simulation reliability.

References:

[1] M.A. Kinch, Fundamentals of Infrared Detector Materials, (SPIE, Washington, 2007) 31-59.  
 [2] D.R. Rhiger, J. Electron. Mater., **40** (2011) 1815-1822.  
 [3] E.H. Steenberg *et al*, Appl. Phys. Lett., **99** (2011) 251110 1-3.  
 [4] K. Mahalingam *et al*, Appl. Phys. Lett., **103** (2013) 061908 1-4.  
 [5] The authors gratefully acknowledge support from MURI Grant W911NF-10-1-0524.

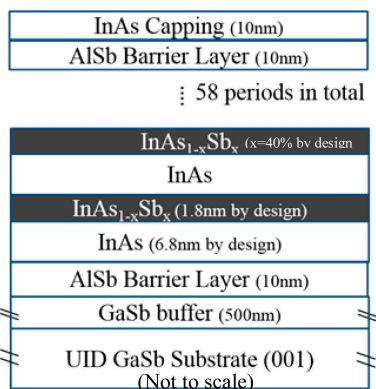


Figure 1. Schematic of T2SL structure.

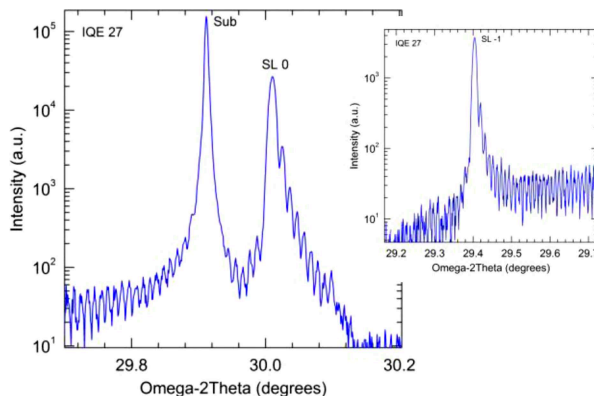


Figure 2. Portion of (004)  $\omega$ - $2\theta$  high resolution XRD pattern.

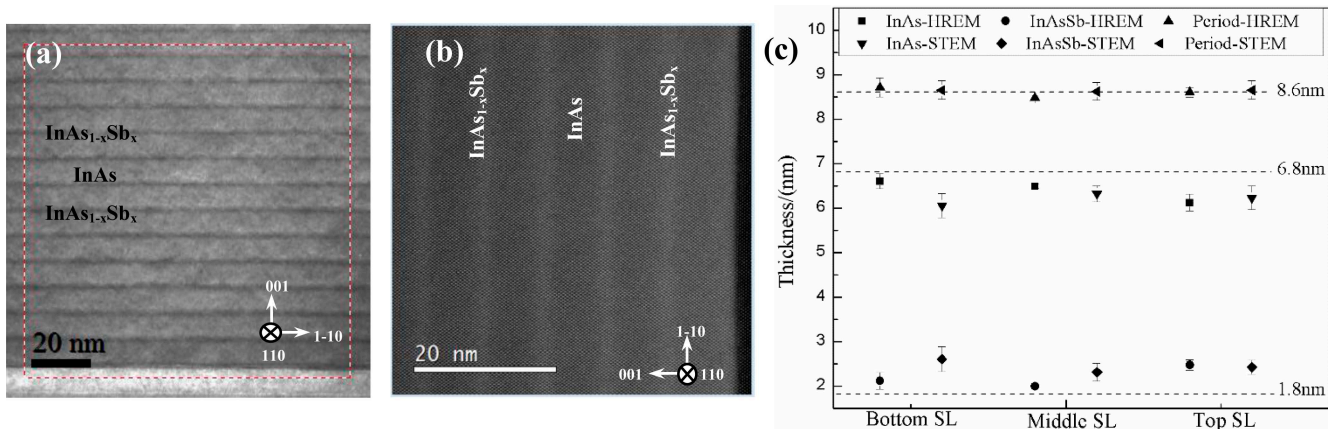


Figure 3. Example (a) HREM and (b) AC-STEM images, and (c) thickness measurement summary.

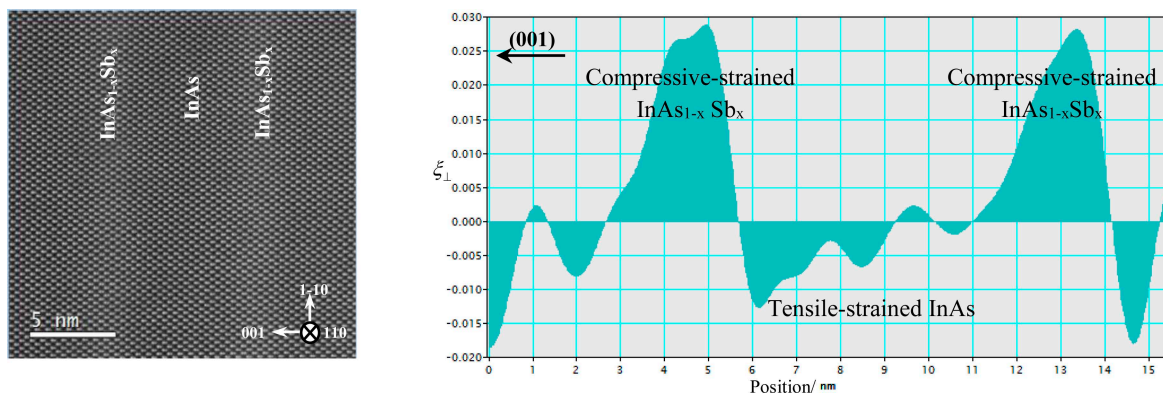


Figure 4. AC-STEM HAADF image and average out-of-plane strain profile from GPA analysis.